*Int. J. Heat Mass Transfer.* Vol. 16, pp. 1513–1525. Pergamon Press 1973. Printed in Great Britain

# MEASUREMENTS OF TRANSIENT HEAT FLUXES AND VAPOUR GENERATION RATES IN WATER

**R. B. DUFFEY, A. J. CLARE, D. H. POOLE, S. J. BOARD and R. S. HALL**
Central Electricity Generating Board, Berkeley Nuclear Laboratories, Berkeley, Gloucestershire, England

(*Received* 16 *May* 1972 *and in revised form* 11 *December* 1972)

**Abstract**—Transient energy transfer processes under conditions of acoustic and high pressure loading have been examined experimentally by the rapid laser heating of metal foils under water. Heat fluxes and vapour layer thicknesses have been deduced for the metal temperature range 100–1000°C with water subcoolings between 20 and 290°C. The data obtained permit a description of the energy transfer processes to be made for a wide range of conditions.

## NOMENCLATURE

$A, B, C, D, E, F, H$, constants of integration;
$c$, velocity of sound;
$G$, gas constant;
$K_1$, constant of proportionality defined in appendix;
$K_3$, constant of proportionality in equation of motion;
$k$, thermal conductivity;
$m$, mass of vapour per unit area;
$P$, pressure;
$Q$, heat flux per unit area;
$R$, effective radius of heated target area;
$s$, specific heat;
$T$, temperature;
$T_{sat}$, saturation temperature;
$t$, time;
$u$, local fluid velocity;
$x$, liquid/vapour boundary displacement;
$\dot{x}, \ddot{x}$, liquid/vapour boundary velocity and acceleration;
$\alpha$, thermal diffusivity ($k/\rho s$);
$\gamma$, coefficient of cubical expansion;
$\delta$, vapour blanket thickness;
$\lambda$, thermal boundary layer thickness;
$\rho$, density;
$\rho_{sat}$, vapour density at saturation temperature;
$\tau$, time scale in heat conduction equations.

Subscripts

$l$, liquid phase;
$v$, vapour phase;
$\infty$, bulk liquid conditions;
$w$, target.

## 1. INTRODUCTION

IT IS known that in thermal explosions pressures of the order of a hundred atmospheres can result from the production of small volumes of vapour [1, 2]. During the early stages of an explosion vapour production will take place under conditions in which expansion is restricted to the volume provided by the compression of the liquid as the pressure wave propagates into the surrounding fluid (acoustic loading). Later, when the pressure wave has been reflected from the free surface expansion will be determined by non-compressive flow according to Newton's second law. The effect of appreciable restriction is the generation of significant pressure.

Several energy transfer processes relevant to thermal explosions have been observed in previous experimental work in an open tank at atmospheric pressure [3]. In order to obtain information on vapour generation rates and heat fluxes under acoustic and high pressure conditions, two further sets of experiments have been performed in which metal targets (typically

0·001 cm thick nickel or 0·002 cm tungsten or tantalum) were heated under water by a pulsed laser at rates of between 1 and 10°C $\mu s^{-1}$ to temperatures of up to 1000°C and at external pressures within the range of 1–100 atm.

## 2. ACOUSTIC AND HIGH PRESSURE CONDITIONS

Consider a vertical column of fluid in a rigid vessel with vapour production uniformly over the base. If the pressure generated is such that any local departure from the normal liquid density is negligible, a plane wave propagates through the column at the bulk acoustic velocity and the equation of motion for the fluid behind the wave becomes [4, 5]:

$$P_v - P_\infty = \rho_l u c_\infty. \tag{1}$$

If the pressure at a point in the system is monitored, then equation (1) permits an estimate to be made of the instantaneous local water velocity until such time as the reflected pressure wave returns (1·3 ms for a 1 m column) provided that the compressibility of the system is effectively that of the fluid. After many reflections, an approximately uniform pressure gradient exists within the column and movement of the whole column may then be described by Newton's laws as applied to a rigid piston.

In order to cover a range of pressures of up to 100 atm to investigate the conditions representative of an explosion a smaller pressurized tank was also used in which transient pressure measurements made at the wall were only of a qualitative nature.

A detailed discussion of the vessel designs is given in the following section.

## 3. EXPERIMENTAL PROCEDURE

The experimental arrangement used for the acoustic loading experiments is illustrated schematically in Fig. 1(a). This comprised a cylindrical column of 1 m length and 6 mm i.d. filled with filtered distilled water, and a foil target mounted near the base.

The system was thoroughly degassed by

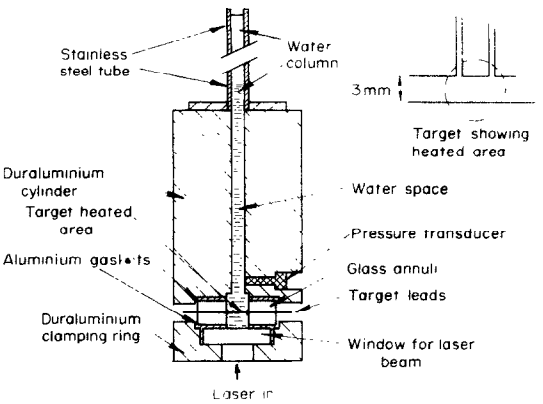


FIG. 1(a). Cross-section of acoustic loading apparatus.

inducing boiling and cavitation at low pressures. and the compressibility checked to be that of water alone by measuring the movement of the water level in a capillary gauge during the application of a gas overpressure. These procedures were sufficient in practice to achieve acoustic loading conditions at water temperatures of up to 80°C. Above this temperature, the evolution of gas at cavities in the vessel wall occurred.

The pressure was measured with a Kistler 603B transducer mounted with its face tangential to the inner wall of the column about 20 mm above the target.

The pressure is due to the combined effects of vapour production at the target and thermal expansion of both the target and the surrounding heated liquid. The heated liquid contributes a fluid velocity over the target area of:

$$\frac{Q\gamma_l}{\rho_l s_l}$$

and during the period of nett vapour production this was calculated to contribute $<10$ per cent of the measured pressure (target expansion accounting for 1 per cent). In the following discussion therefore, the pressure trace is interpreted as being due to motion of a vapour/liquid interface. The velocity of this interface is related to the velocity given by equation (1) in the ratio

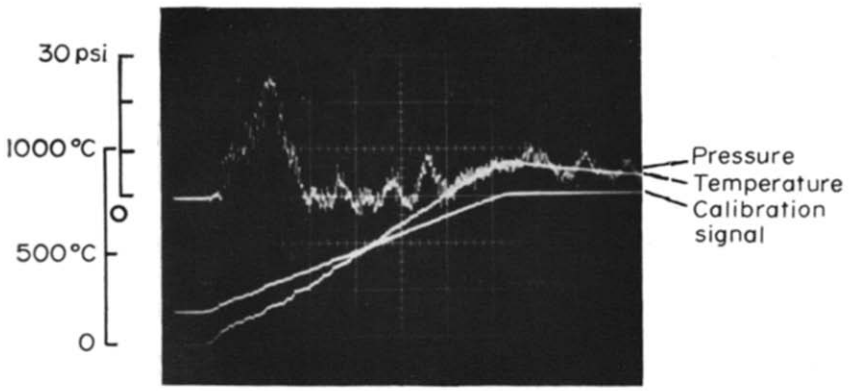


Selected event with a target heated to 1000°C (timescale 50$\mu$s/division)

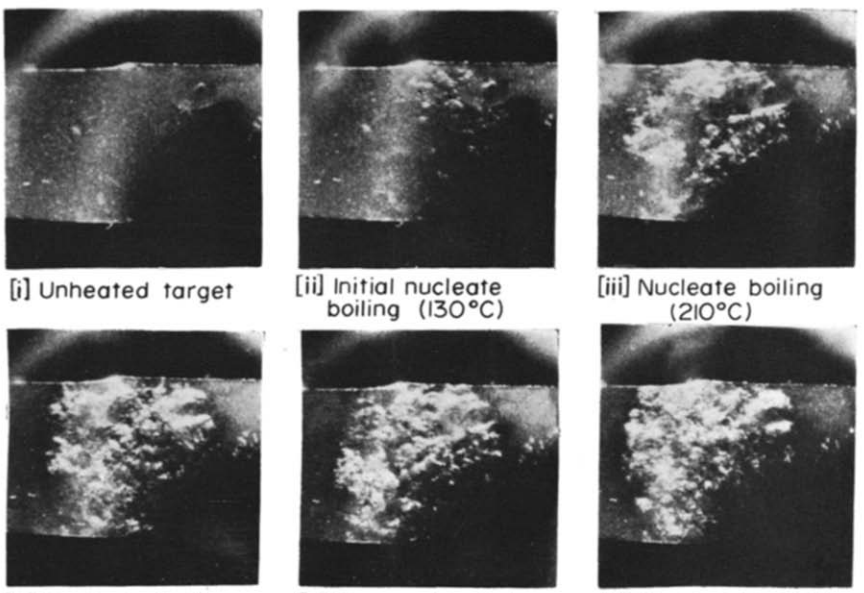


Photographic sequence showing a target heated to 500°C in 300 $\mu$s in 20°C water

FIG. 2. Events under acoustic loading (20°C water).



[*facing page* 1514]

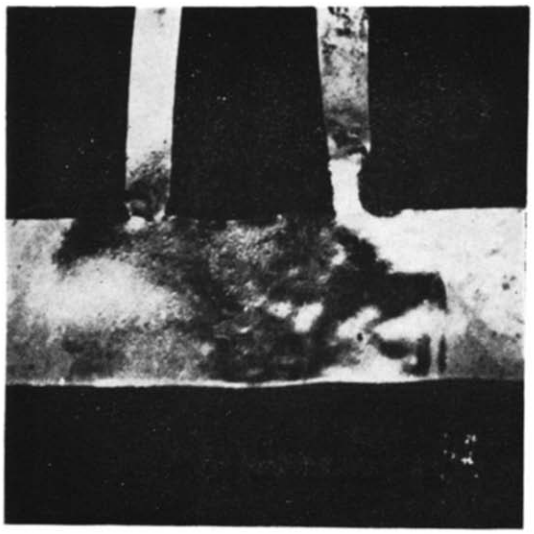

(a) 100 atm

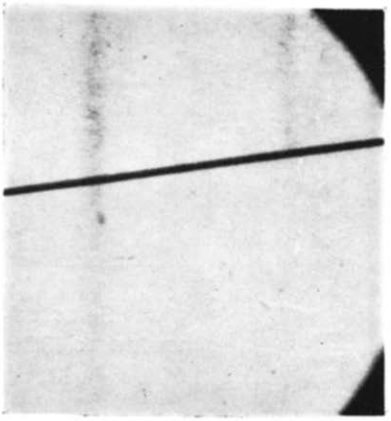

Unheated wire

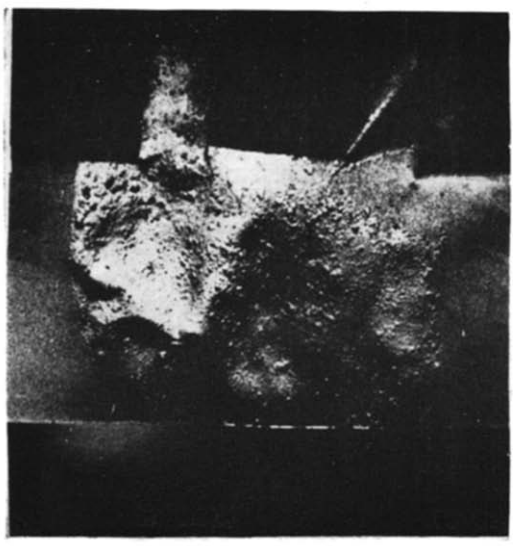

(b) 1 atm

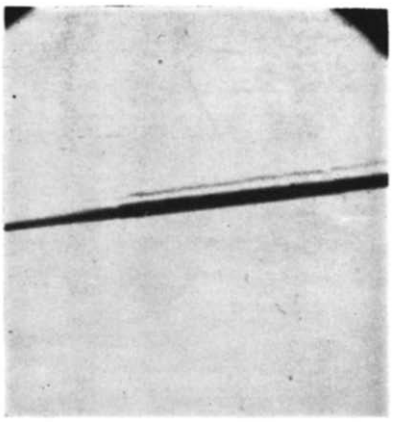

Heated wire 200 $\mu$s after reaching saturation temperature

FIG. 6. Vapour film on a $10^{-3}$cm wire at 100 atm.

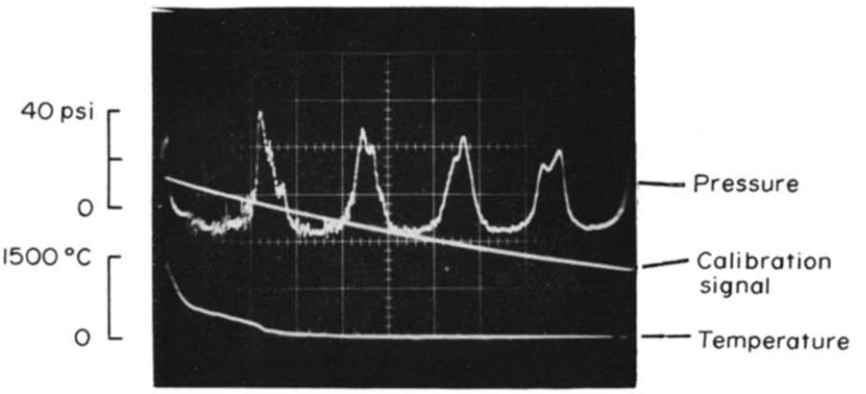


(a) Water column bouncing
(timescale 2 ms/division)

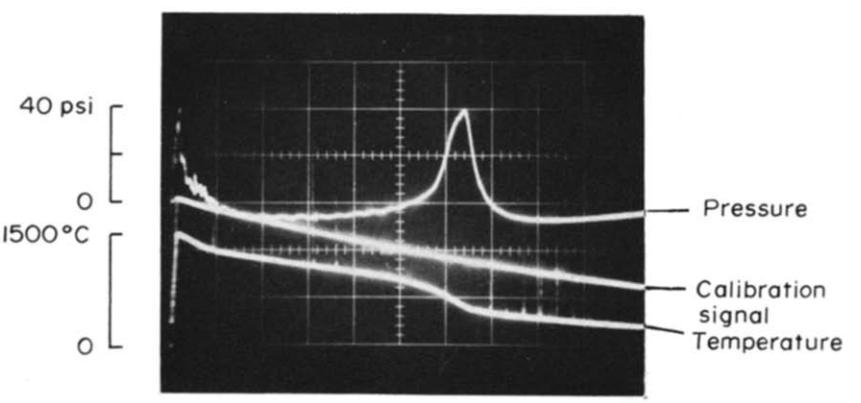


(b) Detail of a first bounce
(timescale 1 ms/division)

FIG. 9. Column bouncing in linear geometry due to gas evolution.

of the areas of tube and of heated target surface, assuming the small volume of water surrounding the target to be incompressible. The average thickness of the vapour layer, its approximate mass and the nett mass generation rate are all obtained from the pressure trace.

The vessel used for the high pressure experiments is illustrated schematically in Fig. 1(b). The water space, of 25 mm dia and length, was filled with degassed distilled water and pressurized over the range of 1–100 atm. The target was positioned in the centre of the vessel by means of ceramic-insulated electrical connections mounted through the wall. Transient pressures produced in this vessel were monitored with a wall-mounted Kistler 603B transducer.

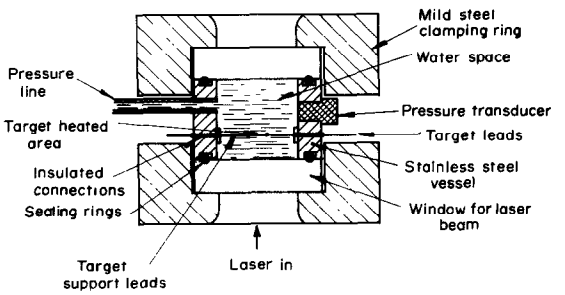


FIG. 1(b). Cross-section of high pressure apparatus.

The metal targets in both vessels were uniformly heated (±20 per cent) over a 3 mm dia area by means of a pulsed ruby laser beam, the mean target temperature being measured to within ±5 per cent by a resistivity technique. The details of these systems and of the methods of data recording and photography have been given elsewhere [3, 6].

The heat fluxes from the target were determined both during and after the heating pulse. During the heating pulse, the fluxes were computed from the difference between the rate of increase of the target temperature and that of a similar target simultaneously heated in air where the heat losses were negligible (typical differences were of the order of $1°C\ \mu s^{-1}$ at a heating rate $\sim 3°C\ \mu s^{-1}$). Both targets were initially heated simultaneously in air to provide a calibration factor, and the integrated output of a calibrated photodiode was used as a secondary standard. For the cooling cycle, the fluxes were obtained directly from the target cooling rate. The effect of temperature variations over the target would be expected to be most important for regions of decreasing flux with increasing temperature: however the results (e.g. Fig. 3(c)) where the flux is observed to fall by an order of magnitude within $\sim 50°C$ indicate that good temperature uniformity must exist even in this region. Heat fluxes deduced from repeated events have a significant scatter (±20 per cent) and therefore heat flux versus temperature plots are obtained by averaging the results of many events (typically 10–20). The errors in the heating cycle flux measurements are larger (±30 per cent) than those in cooling cycle measurements (±10 per cent) mainly due to the differencing method, though also due to irregular fluctuations in the mean laser power.

The results are summarized in the next section, and discussed in detail in later sections.

## 4. SUMMARY OF RESULTS

### 4.1 *Acoustic loading apparatus*

Figure 2 shows a selected event record illustrating the processes occurring under acoustic loading and giving data on incident (absorbed) energy, target temperature and local pressure, together with a photographic sequence showing the target heated to 500°C in 300 μs at 80°C sub-cooling at atmospheric pressure.

Results were taken at subcoolings of 80°C, 40°C and 20°C and with heating rates between 1 and $5°C\ \mu s^{-1}$.

The flux during heating under acoustic loading is shown in Figs. 3(a), (b) and (c). Each point represents the average of measurements from $\sim 20$ events. Any variation of flux with heating rate was within the scatter in the data. Peak fluxes lie between 2 and 4·5 $kWcm^{-2}$ at temperatures between 300°C and 400°C.

In Figs. 4(a) and (b), typical curves are given

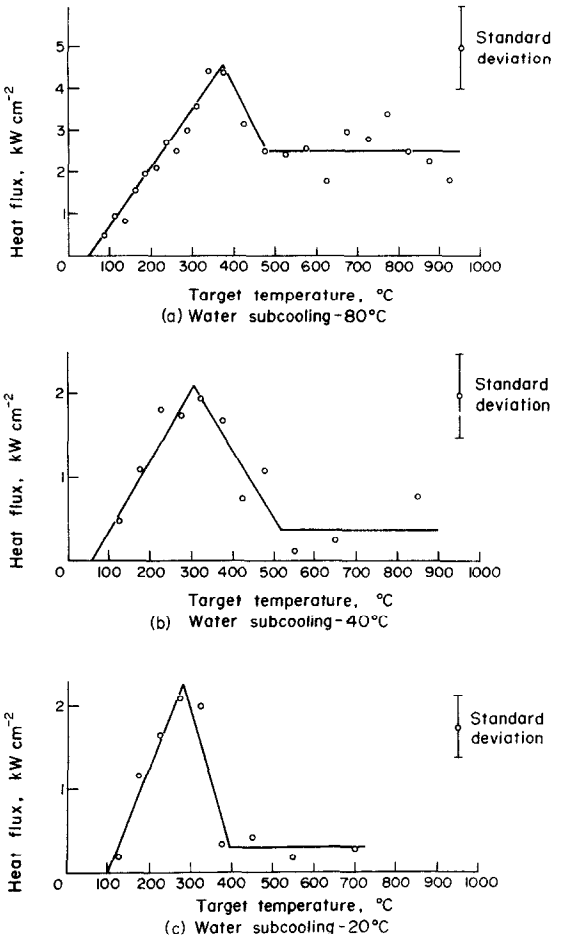


FIG. 3. Heat fluxes in acoustic conditions.
(a) 20°C Water
(b) 60°C Water
(c) 80°C Water

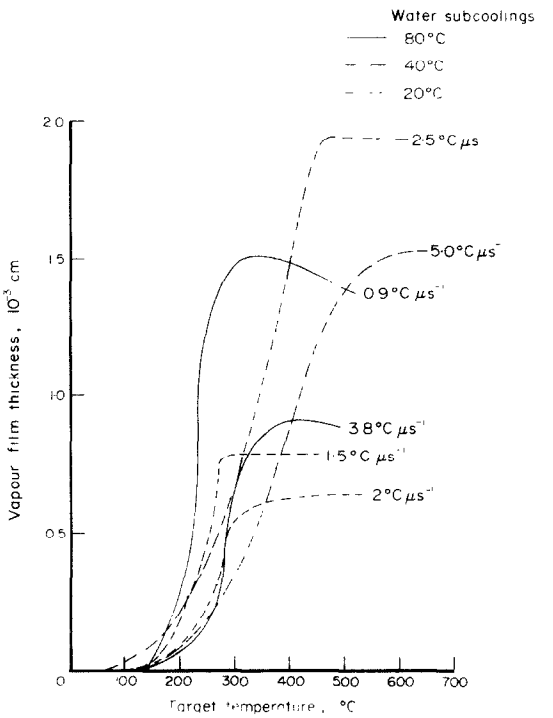


FIG. 4(a). Vapour blanket thickness.

of the variation of average thickness and mass respectively of vapour blankets as a function of target temperature. The nett vapour mass generation rates are plotted in Fig. 4(c) as a function of target temperature.

The fraction of the flux from the target required to produce the observed maximum nett vapour generation rates ($\dot{m}L/Q$) increases with heating rate, being 0·08 per cent at 0·9°C μs$^{-1}$ and 4 per cent at 3·8°C μs$^{-1}$ at 20°C, and appears to show a maximum ($\sim$ 17 per cent) at moderate subcoolings.

The fraction of flux from the target which does external mechanical work through vapour expansion ($P_v\dot{\delta}/Q$) for these events also increases with heating rate and appears to show a maximum with water temperature, varying from $3 \times 10^{-3}$ at 3·8°C μs$^{-1}$ in 20°C water to $1{\cdot}5 \times 10^{-2}$ at 5°C μs$^{-1}$ in 60°C water.

Although there is some evidence of periodicity in the pressure traces, this is not associated with distinct temperature steps nor does it show any systematic variation with subcooling. Hence, there is no evidence for a coherently oscillating vapour blanket as observed in transition boiling in open vessels cf. [3]).

### 4.2 *High pressure apparatus*

The average fluxes during the heating cycle in the high pressure apparatus at 20°C are shown in Figs. 5(a) and 5(b) for water under external pressures of 20 and 100 atm respectively. The

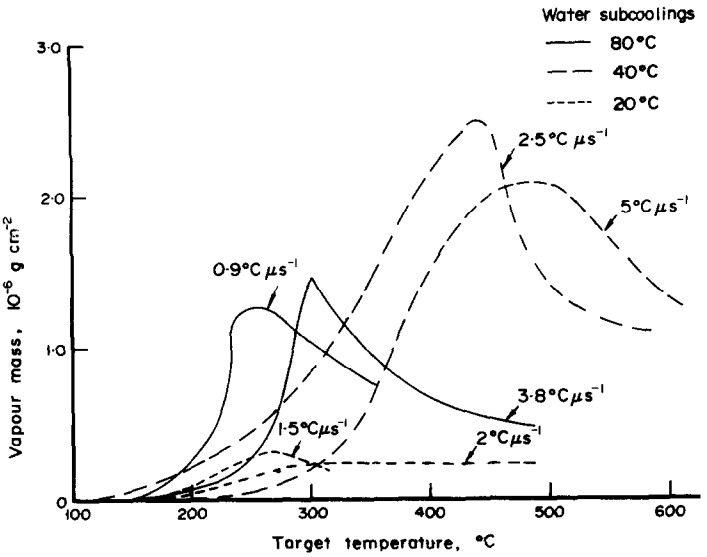


FIG. 4(b). Vapour blanket mass.

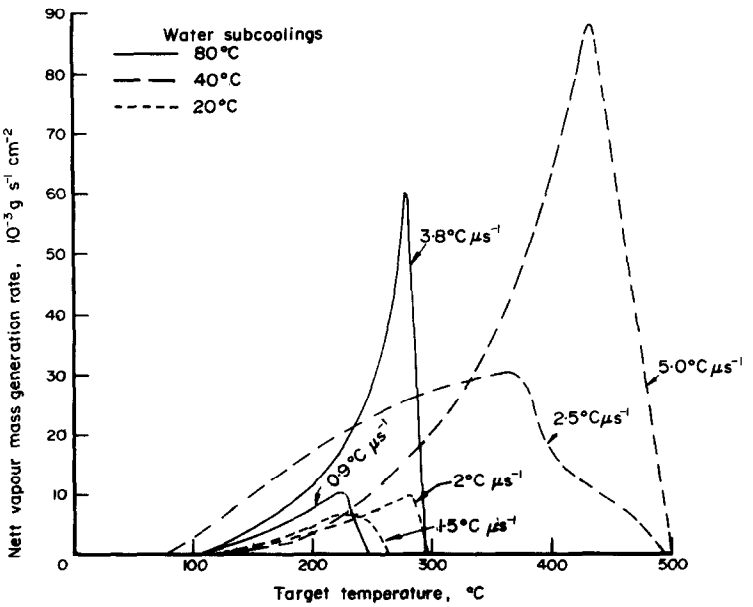


FIG. 4(c). Nett vapour mass generation rate.

saturation temperatures corresponding to these pressures are approximately 200°C and 300°C.

The behaviour at 1 atm is the same as that described previously for an open vessel [3].

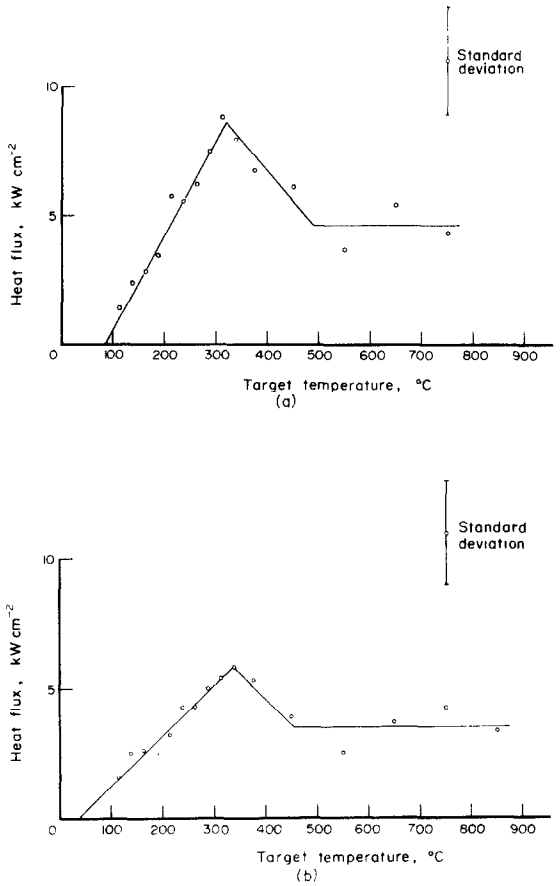


FIG. 5. Heat fluxes at high pressure in 20°C water.
(a) 20 atm
(b) 100 atm

Photographs of the target taken at pressures of 20 and 100 atm show no vapour below the saturation temperature and discrete vapour bubbles characteristic of nucleate boiling immediately above. At higher temperatures a thin vapour blanket is formed. A photograph of such a blanket on a target at 500°C with an external pressure of 100 atm which shows well-defined edges and superimposed bubble-like irregularities is given in Fig. 6(a). It can be seen that the size of the irregularities is significantly less than on a blanket at the same target temperature at 1 atm, a typical photograph of which is given in Fig. 6(b). An estimate of the average blanket thickness may be obtained from the assumption that the size of the observed irregularities on the surface of the film is of the same order as its depth. On this basis the thickness of the vapour blanket at 100 atm is $\sim 10^{-3}$ cm.

An unambiguous measurement of the thickness has been obtained using heated wires. A film thickness of 4 $(\pm 2).10^{-4}$ cm has been measured from photographs of a wire of $10^{-3}$ cm dia at 600°C (about 200 μs after reaching the saturation temperature) as shown in Fig. 6(c). The production of a film of this thickness in this time implies an average vapour generation rate of 240 W cm$^{-2}$ ($\sim 5$ per cent of the flux)—this is comparable to the acoustic loading measurements at 80°C subcooling at similar heating rates.

## 5. THE ENERGY TRANSFER REGIONS

From the results presented above we may define the distinct regions of energy transfer in transient boiling (shown schematically in Figs. 7(a) and (b)) as follows:

(a) Liquid conduction region, for target temperatures less than the saturation temperature, in which the dominant energy transfer mechanism is transient conduction in the liquid.

(b) Nucleate boiling region commencing at target temperatures greater than the saturation temperature and characterized by the growth of discrete vapour bubbles on the target.

(c) Intermediate boiling region, defined as the region where the average flux decreases with increasing target temperature (corresponding to conventional transition boiling).

(d) High temperature region, above 500°C, in which the flux is independent of target temperature, and a thin, irregular vapour layer covers the target (corresponding to conventional film boiling).

These regions are discussed in detail in the following sections.

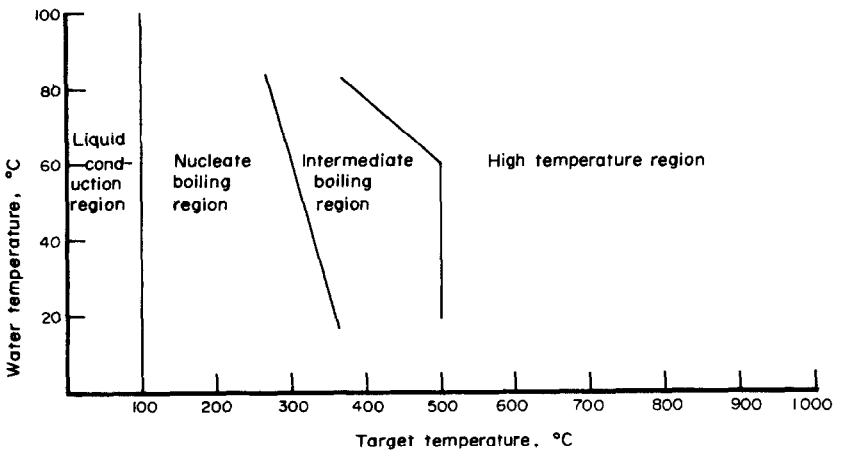


FIG. 7(a). Energy transfer regions under acoustic loading.

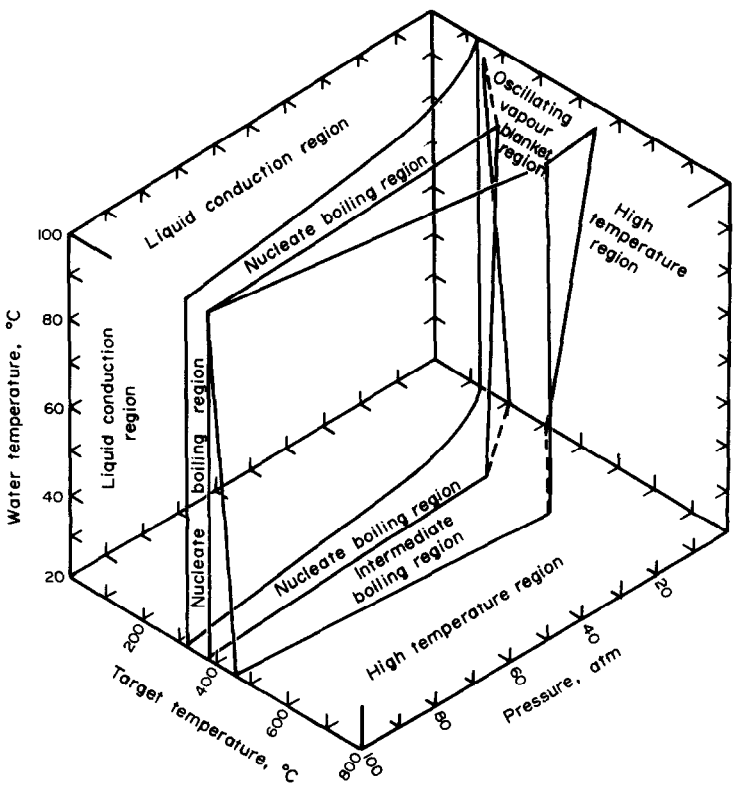


FIG. 7(b). Energy transfer regions in open vessel and pressurized geometries.

## 6. THE NUCLEATE AND INTERMEDIATE BOILING REGIONS

In the high pressure apparatus the increased saturation temperature results in an extended non-boiling transient conduction region. At a pressure of 100 atm the nucleate boiling is restricted to a temperature interval ($T_{peak} - T_{sat}$) of about 30°C and the peak flux is lower than in the 20 atm case.

At temperatures below the saturation temperature, the flux can be accounted for by transient conduction to the liquid. Above the saturation temperature, and at a given subcooling, the peak fluxes are greater than those determined for transient pool boiling at lower pressures [3, 7, 8].

The results of vapour production measurements in the nucleate boiling region (i.e. an increase of nett mass generation rate with heating rate at a given subcooling) may be interpreted in terms of the now generally accepted microlayer theory (e.g. [9, 10]). It is observed that the flux is independent of heating rate, and hence the evaporation rate for the microlayers on the target should also be independent. However, the condensation rate will lag behind the evaporation rate until the vapour bubbles have grown sufficiently. Thus, at high heating rates, evaporation will initially greatly exceed condensation and the nett vapour generation rate will thus be large.

The observed rapid increase of heat flux with temperature would also be expected on the microlayer theory (as in steady boiling) since the temperature gradient across the microlayer increases as (a) the foil temperature rises, (b) the layer thins by evaporation and (c) new bubbles are formed with thinner layers at higher superheats, possibly within previously existing layers. (Typical bubble growth timescales are $\sim 20$ μs compared with 200 μs heating time.) Continued evaporation and thinning must cause dryout before the foil temperature reaches the critical temperature of water (374°C) unless supercritical pressures can exist locally. In these experiments, the occurrence of dryout is indicated by a falling heat flux (see Fig. 3) as the vapour is increasingly replacing the liquid contiguous with the target.

In the intermediate or transition boiling region under acoustic loading, the non-occurrence of coherent oscillations of the vapour blanket is of particular significance. The simple theory of vapour blanket movement developed in the Appendix shows that small departures from an assumed equilibrium vapour blanket thickness are damped under acoustic loading conditions where the pressure is proportional to the displacement velocity. Therefore coherent oscillations would not be expected until pressure reflection from the free surface established noncompressive motion of the water column (see also section 8).

## 7. THE HIGH TEMPERATURE REGION

The conditions of high target temperature at high pressure, and hence high subcooling, are directly relevant to thermal explosions.

The flux in the high temperature region ($T_w > 500$°C) increases with increasing subcooling as shown in Fig. 8, which contains results from both the acoustic loading and pressurized apparatus.

The straight lines shown in Fig. 8 represent the theoretical transient conduction loss, $Q_l$, across a thermal diffusion boundary layer in the water adjacent to the vapour blanket, where the liquid/vapour interface is at the saturation temperature. Under these conditions,

$$Q_l = \frac{k_l(T_{sat} - T_\infty)}{\lambda} \qquad (2)$$

where $\lambda = (\pi\alpha t)^{\frac{1}{2}}$.

The lines shown are calculated from equation (2) using values for $t$ of 200 and 300 μs, which correspond to the times during and after the period when the foil was being heated.

It may be seen that the fluxes lie above the transient conduction line by up to a factor of three. Since radiation can be neglected, heat transfer in the water is by conduction or convection, so that significant increases above the

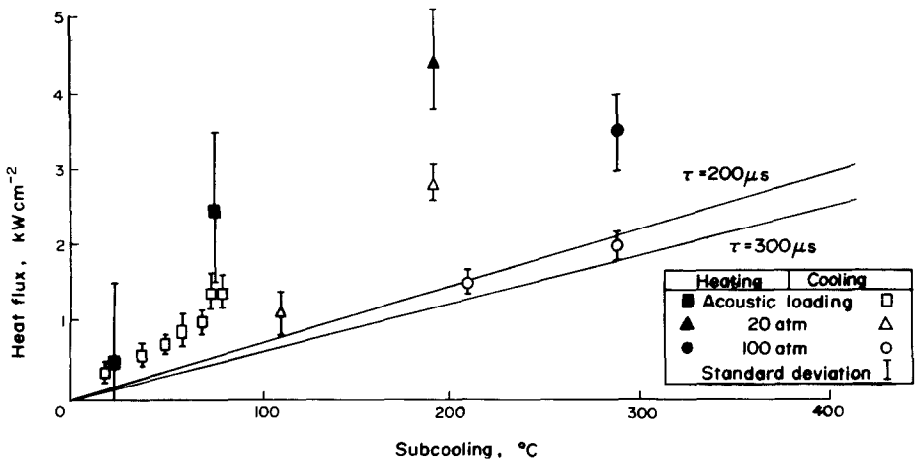


FIG. 8. Heat flux/subcooling in the high temperature region.

transient conduction flux must be due to convection, presumably excited by turbulence at the vapour/liquid interface.

The above considerations lead to the postulate that if the target is maintained above the saturation temperature and that there is local pressure equilibrium, then the total flux to the water cannot be less than that due to a thermal diffusion boundary layer with a plane interface maintained at the saturation temperature.

The observed fluxes under acoustic loading (Fig. 3(c)) at low subcoolings are consistent with conduction across a pure laminar vapour film of the measured thickness, thus:

$$Q_v = \frac{k_v(T_w - T_{sat})}{\delta} \qquad (3)$$

which predicts $Q_v = 300\ \mathrm{W\,cm^{-2}}$ for a 500°C target at 20°C subcooling and $\delta \sim 6 \times 10^{-4}$ cm (see Fig. 4(a)).

However, the observed fluxes at high subcoolings are up to an order of magnitude greater than given by equation (3). This indicates that at high subcoolings liquid exists closer to the target than would be expected from the average vapour blanket thickness measurements; that is, the blanket may be in the form of a two-phase layer as suggested previously [3].

## 8. SOME REMARKS ON THE EFFECTS OF GAS UNDER ACOUSTIC LOADING

Permanent gas was evolved occasionally from the water column in the acoustic loading apparatus during experiments involving water temperatures above 70°C or 80°C and was also evolved from targets heated to temperatures in excess of 1000°C. The gas from the water was observed to be in the form of a small number of discrete bubbles on the walls which would therefore influence the effective loading of the system, whereas that from the target was injected into the vapour blanket and hence might be expected to influence the energy transfer processes directly. These effects are described separately.

Evolution of gas from the water was usually eliminated by the procedures outlined in section 3. However, in early attempts to reach low subcoolings, a few discrete bubbles appeared on the walls of the vessel in the region of the target. The effect of these bubbles was that the energy transfer processes immediately became similar to those characterizing open geometry. In particular, the oscillating vapour blanket region occurred over the same target temperature range and with the same step heat fluxes as in the experiments discussed by Board *et al.* [3]. The

nearest bubbles, approximately 6 mm distant from the target, were of diameter about 1 mm.

This effect may be understood by considering that the bubbles provide a nearby free surface for pressure relief, hence reducing the effective length of the water piston coupled to movements of the vapour blanket and providing inertial instead of acoustic loading. This phenomenon may be relevant to inter-particle effects in thermal explosions.

Permanent gas evolution from the target was found to cause anomalously large pressure pulses which implied an order-of-magnitude increase in boundary displacement. The evolution was found to occur increasingly above a temperature characteristic only of the target material (e.g. tantalum $\sim 1000°C$, nickel $\sim 1400°C$, tungsten $\sim 1400°C$, molybdenum $\sim 1500°C$). However, the evolution of gas did not markedly affect the heat fluxes (near 5 kW $cm^{-2}$) at very high temperatures ($>1000°C$) which suggests that the energy transfer process is relatively insensitive to blanket thickness for thicknesses $<10^{-2}$ cm; this is not inconsistent with the two-phase model postulated in section 7 to account for the energy transfer in the high temperature region.

The permanent gas evolved from the target, unlike the condensable vapour, remained constrained at relatively high pressure ($\sim 10$ atm) until relief was provided by motion of the whole water column. This motion markedly reduced the heat flux when the blanket thickness became greater than $10^{-2}$ cm. The subsequent motion of the column consisted of a series of up to 10 bounces (see Fig. 9(a)), with sharp pressure pulses and increased heat flux occurring whenever the column approached the hot target. The detail of one of these pressures pulses is shown in Fig. 9(b), with the column approaching to within $10^{-2}$ cm of the target. The maximum heat fluxes observed during this approach were comparable to those obtained in open geometry experiments.

Similar bouncing motions have been observed in experiments with much greater heated areas [5, 11–14], where the vapour production could maintain the pressure for long enough to produce whole column motion.

## 9. CONCLUSIONS

Transient heat fluxes and vapour production rates have been measured as functions of subcooling and target temperature under acoustic loading and under external pressures of up to 100 atm. They confirm the existence under conditions relevant to thermal explosions of several distinct energy transfer regions, similar to those found in earlier work in an open vessel [3].

The nucleate boiling region has been shown to extend from the saturation temperature nearly to the critical temperature of water, with peak fluxes of between 5 and 10 kW $cm^{-2}$ depending on loading conditions. The main effect of high pressures is to restrict the interval between the saturation and critical temperatures over which nucleate boiling can occur. Under acoustic loading, the vapour blanket was shown to be stable against coherent oscillations of the type observed in an open vessel.

In the high temperature region ($>500°C$), fluxes were found in general to be up to three times greater than those which would be supported by transient conduction in the liquid, assuming a plane liquid/vapour interface at the saturation temperature. The hypothesis was advanced that fluxes above this level were due to turbulence in the thermal boundary layer. It was postulated that the flux required to maintain a plane liquid/vapour interface at the saturation temperature against transient conduction formed an absolute lower limit to the flux lost by a target above the saturation temperature.

Vapour production rates measured under acoustic loading conditions showed that the maximum rate of vapour mass generation increased rapidly with target heating rate, reaching about 200 W $cm^{-2}$ (10–20 per cent of the total flux) at a heating rate of $5° \mu s^{-1}$. In the high temperature region, the average vapour blanket

thickness at high subcoolings (>20°C) was too great to support the observed flux by conduction in pure vapour; it is suggested that the additional mechanism of evaporation of liquid in the vapour near the target is important. At low subcoolings (20°C) the observed flux can be adequately accounted for by conduction across a plane vapour blanket.

## ACKNOWLEDGEMENT

This paper is published by permission of the Central Electricity Generating Board.

## REFERENCES

1. R. W. MILLER, A. SOLA and R. K. MCCARDELL, Report of the SPERT 1 destructive test program on an aluminium, plate-type, water-moderated reactor, U.S.A.E.C. Report IDO-16883 (1964).
2. R. W. WRIGHT, Review of the SPERT 1D destructive test, U.S.A.E.C. Report STL 372-30, 24–30 (1965).
3. S. J. BOARD, A. J. CLARE, R. B. DUFFEY, R. S. HALL and D. H. POOLE, An experimental study of energy transfer processes relevant to thermal explosions, *Int. J. Heat Mass Transfer* **14**, 1631–1641 (1971).
4. R. H. COLE, *Underwater Explosions*, pp. 18–20. Dover, New York (1965).
5. R. W. WRIGHT and L. B. WENTZ, Summary of the process of transient thermal pressure generation, U.S.A.E.C. Report STL 373-50, 15 (1966).
6. A. J. CLARE and W. N. WALKER, A high-speed multichannel data acquisition system using a small digital computer, C.E.G.B. Report RD/B/N1683 (1970).
7. W. B. HALL and W. C. HARRISON, Transient boiling of water at atmospheric pressure, Proc. 3rd Int. Heat Transfer Conf., I.Mech.E., Chicago, pp. 186–192 (1966).
8. F. TACHIBANA, M. AKIYAMA and H. KAWAMURA, Heat transfer and critical heat flux in transient boiling, (1)—an experimental study in saturated pool boiling, *J. Nucl. Sci. Tech.* **5**, 117–126 (1968).
9. F. D. MOORE and R. B. MESLER, The measurement of rapid temperature fluctuations during nucleate boiling of water, *A.I.Ch.E.Jl* **7**, 620–624 (1961).
10. M. G. COOPER and A. J. P. LLOYD, The microlayer in nucleate pool boiling, *Int. J. Heat Mass Transfer* **12**, 895–913 (1969).
11. R. W. WRIGHT, Kinetic studies of heterogenous water reactors, U.S.A.E.C. Report STL 6306 1-32 (1963).
12. R. W. WRIGHT, Pressure pulses in rapid transient boiling, *Trans. Am. Nucl. Soc.* **6**, 338–339 (1963).
13. L. B. WENTZ, In-pile capsule measurements of transient steam-void growth and collapse, U.S.A.E.C. Report STL 372-30, 7-23 (1965).
14. H. UCHIDA and T. YAMURA, Analysis of pressure pulses produced in a water channel by rapid heating, *Nuclear Safety* **11** (1), 12–19 (1970).

## APPENDIX

### *Vapour Blanket Stability*

Using the arguments and assumptions of the appendix of the previous paper (Board *et al*, 1971), the heat flux from the target is taken to follow a conductivity law

$$Q \propto \frac{1}{\delta} = \frac{K_1}{\delta} \tag{1}$$

so that the nett vapour generation rate caused by a small displacement $x$ from the blanket equilibrium position is

$$\dot{m} = -\frac{K_1 x}{\delta^2 L} \tag{2}$$

$$\doteq \delta \dot{\rho}_v + \dot{x}\rho_{sat}. \tag{3}$$

For a perfect gas, small changes along the saturation curve may be approximated by

$$\dot{P}_v \doteq \dot{\rho}_v G T_\infty. \tag{4}$$

Now the equation of motion for acoustic conditions is

$$P_v - P_\infty = \rho_l c_\infty \dot{x} \tag{5}$$

$$\text{i.e. } \dot{P}_v = \rho_l c_\infty \ddot{x}. \tag{6}$$

Equations (2), (3), (4) and (6) may be combined to give a linear differential equation in $x$,

$$\frac{\delta \rho_l c_\infty}{G T_\infty} \ddot{x} + \rho_{sat} \dot{x} + \frac{K_1}{\delta^2 L} x = 0 \tag{7}$$

with solution

$$x = D \exp C_1 t + E \exp C_2 t \tag{8}$$

where $C_1$ and $C_2$ are given by

$$C_{1,2} = -\frac{\rho_{sat} G T_\infty}{2\delta \rho_l c_\infty} \pm \frac{1}{2\delta \rho_l c_\infty} \left[ (\rho_{sat} G T_\infty)^2 - \frac{4 \rho_l c_\infty G T_\infty K_1}{L\delta} \right]^{\frac{1}{2}}.$$

Comparing the magnitude of the terms inside the square root using the typical values,

$\rho_{sat} G T_\infty \simeq P_{sat} \simeq 2$ atm

$\rho_l = 1$ g cm$^{-3}$

$c_\infty = 1{\cdot}5 . 10^5$ cm s$^{-1}$

$G = 0{\cdot}46\ \mathrm{J\,g^{-1}\,^{\circ}K^{-1}}$

$T_\infty \simeq 300^{\circ}\mathrm{K}$

$\delta \simeq 10^{-3}$ (from Fig. 4(a))

$Q \simeq 10^3\ \mathrm{W\,cm^{-2}}$ (from Fig. 3)

$K_1 = Q \times \delta$(from equation (1))

$= 1\ \mathrm{W\,cm^{-1}}$

$L = 2{\cdot}3 \cdot 10^3\ \mathrm{Jg^{-1}}$

it can be shown that

$$\frac{4\rho_l c_\infty GT_\infty K_1}{L\delta} \gg (\rho_{sat} GT_\infty)^2.$$

Hence the solution (8) of equation (7) may be written

$$x = \exp - \frac{\rho_{sat} GT_\infty}{2\delta\rho_l c_\infty} t \left[F \cos\left(\frac{GT_\infty K_1}{L\delta^3\rho_l c_\infty}\right)^{\frac{1}{2}} t + H \sin\left(\frac{GT_\infty K_1}{L\delta^3\rho_l c_\infty}\right)^{\frac{1}{2}}\right]. \quad (9)$$

This solution represents a damped harmonic oscillation with frequency

$$\frac{1}{2\pi}\left(\frac{GT_\infty K_1}{L\delta^3\rho_l c_\infty}\right)^{\frac{1}{2}}$$

and damping time constant

$$\frac{2\delta\rho_l c_\infty}{\rho_{sat} GT_\infty} = \frac{2\delta\rho_l c_\infty}{P_{sat}}$$

This may be compared with the solution for inertial loading, which is, correcting an error in sign in the earlier paper,

$$x = A\exp(s_1 + s_2)t + \left[B\cos\frac{\sqrt{3}}{2}(s_1 - s_2)t + C\sin\frac{\sqrt{3}}{2}(s_1 - s_2)t\right]\exp -(s_1 + s_2)t$$

where

$$s_1 = \left\{\frac{-K_1 GT_\infty}{2\delta^3\rho_l K_3 RL}\left[-1 + \sqrt{\left(1 + \frac{4\rho_{sat}{}^3 GT_\infty \delta^3 L^2}{27K_1^2\rho_l K_3 R}\right)}\right]\right\}^{\frac{1}{3}}$$

$$s_2 = \left\{\frac{-K_1 GT_\infty}{2\delta^3\rho_l K_3 RL}\left[1 + \sqrt{\left(1 + \frac{4\rho_{sat}{}^3 GT_\infty \delta^3 L^2}{27K_1^2\rho_l K_3 R}\right)}\right]\right\}^{\frac{1}{3}}.$$

This represents a harmonic oscillation whose amplitude grows with time, since $-(s_1 + s_2)$ is always positive.

Thus in inertial loading conditions, the vapour blanket is unstable, i.e. a perturbation will cause an oscillation which grows, whereas under acoustic loading oscillations are damped and the blanket is stable.

## MESURE DU FLUX DE CHALEUR TRANSITOIRE ET DES TAUX DE GENERATION DE VAPEUR DANS L'EAU

**Résumé**—Les mécanismes de transfert d'énergie transitoire sous les conditions de charge de pression acoustique ou élevée ont été examinés expérimentalement par échauffement lazer rapide de feuilles métalliques dans l'eau. Les flux thermiques et les épaisseurs de la couche de vapeur ont été déterminés pour un domaine de température du métal entre 100 et 1 000°C avec des sous-refroidissements de l'eau entre 20 et 290°C. Les résultats obtenus permettent une description des procédés de transfert d'énergie pour un large domaine de conditions.

## MESSUNGEN INSTATIONÄRER WÄRMESTRÖME UND DAMPFERZEUGUNGSGESCHWINDIGKEITEN IN WASSER

**Zusammenfassung**—Instationäre Energieübertragungsprozesse bei akustischer und Hochdruck-Beeinflussung wurden experimentell untersucht mit Hilfe einer Schnellaufheizung einer Metallfolie in Wasser mit einem Laserstrahl. Wärmeströme und Dampfschichtdicken werden ermittelt für Metalltemperaturen von 100–1000°C bei einer Wasserunterkühlung zwischen 20 und 290°C. Die erhaltenen Daten gestatten die Beschreibung der Energieübertragungsprozesse in einem grossen Bereich.

## ИЗМЕРЕНИЕ НЕСТАЦИОНАРНЫХ ТЕПЛОВЫХ ПОТОКОВ И СКОРОСТЕЙ ПАРООБРАЗОВАНИЯ В ВОДЕ

**Аннотация**—Методом быстрого лазерного нагрева металлической фольги под водой экспериментально исследовались процессы нестационарного энергопереноса в условиях акустической нагрузки и высокого давления. Тепловые потоки и толщина слоя пара измерялись в диапазоне изменения температуры металла от 100 до 1000°С и водяного хладоагента от 20 до 290°С. Температурные данные позволяют описать процессы энергопереноса в широком диапазоне изменения параметров процесса.